On the Instrument-Dependent Appearance of Ion Dissociation Events in Atom Probe Tomography Mass Spectra*

Benjamin W. Caplins[a,*], Ann N. Chiaramonti[a], Jacob M. Garcia[a], Luis Miaja-Avila[b], Kayla H. Yano[c], Daniel K. Schreiber[c], Joseph H. Bunton[d]

[a] *National Institute of Standards and Technology, Applied Chemicals and Materials Division, Boulder, CO, 80305, USA*
[b] *National Institute of Standards and Technology, Applied Physics Division, Boulder, CO, 80305, USA*
[c] *Pacific Northwest National Laboratory, Energy and Environment Directorate, Richland, WA, 99354, USA*
[d] *CAMECA Instruments Inc., Madison, WI, 53711, United States*

Abstract

The successful application of atom probe tomography (APT) relies on the accurate interpretation of the mass spectrum (*i.e.* m/z histogram) from a sample. Some materials yield mass spectra that are amenable to a straightforward peak assignment/ranging, however, there are many materials that produce mass spectra with features that defy simple interpretation. One such example is Ga_2O_3 which yields mass spectra containing several broad and difficult to interpret features. Herein, we study the $GaO^{2+} \rightarrow O^{1+} + Ga^{1+}$ dissociation and we explain how this dissociation process gives rise to broad and previously unassigned features in the mass spectrum. Trajectory simulations are performed for the dissociation reaction utilizing realistic electrostatic models and compared to experiments using commercially available straight flight and reflectron based local electrode (LE) APT instruments. It is shown that the appearance of these features is strongly dependent on the specific design of the time-of-flight (ToF) mass analyzer. We explore how various experimental parameters can affect the appearance of the dissociation process in the one-dimensional (1D) mass spectrum and in the two-dimensional (2D) correlation histogram. While the focus of this work is on a particular dissociation process related to Ga_2O_3, the understanding gained in the course of these simulations and experiments should be applicable to the interpretation of dissociation processes in other materials.

Keywords: atom probe tomography; field ion microscopy; ion trajectory simulation; dissociation; gallium oxide; time-of-flight mass analyzer

1. Introduction

Atom probe tomography (APT) utilizes a field ion point projection microscope in combination with a time-of-flight (ToF) mass analyzer to map the three-dimensional structure of nanoscale specimens at the atomic scale.[1–4] As the technique is based on a ToF mass analyzer, it inherits the assumptions associated with that technique. Notably, in the most basic implementation, a ToF mass analyzer assumes that at time $t = 0$ (*i.e.* when the voltage or optical pulse is incident on the specimen) an ion is instantaneously accelerated to a known amount of kinetic energy by an electrostatic potential difference, traverses a field-free flight tube of known length at a constant velocity, and strikes a microchannel plate (MCP) at a time $t = ToF$. This then leads to Eq. 1 relating the ToF to the ion m/z.[1]

$$\frac{m}{z} = \frac{2eV_{DC}}{L^2} ToF^2 \tag{1}$$

In a practical experiment, L is given by distance from the specimen apex to the MCP and V_{DC} is the voltage drop that accelerates the ion to the MCP, leaving ToF as the only observable (e is the charge on an electron).

If a molecular 'parent' ion dissociates at a time $t_d > 0$ (*i.e.* after it is emitted from the tip) then the resulting 'daughter' ions will strike the MCP and a ToF for each daughter ion will be recorded (assuming a perfect detection quantum efficiency).[5] This process is depicted in Fig. 1a for the $GaO^{2+} \rightarrow O^{1+} + Ga^{1+}$ dissociation studied herein. However, the application of Eq. 1 will yield incorrect values for the m/z for these dissociative events since the

*Commercial equipment, instruments, or materials are identified only in order to adequately specify certain procedures. In no case does such identification imply recommendation or endorsement by the National Institute of Standards and Technology, nor does it imply that the products identified are necessarily the best available for the purpose.

*Corresponding Author
Email address: benjamin.caplins@nist.gov (Benjamin W. Caplins)

[1] In practice Eq. 1 should be regarded only as a very convenient approximation since the acceleration of the ion is never instantaneous, the flight tube is rarely field-free, and the path of the ion is not, in general, linear. The computation of m/z from real ToF data is typically done in a slightly *ad-hoc*, albeit very practical, manner with numerous free parameters.[2]

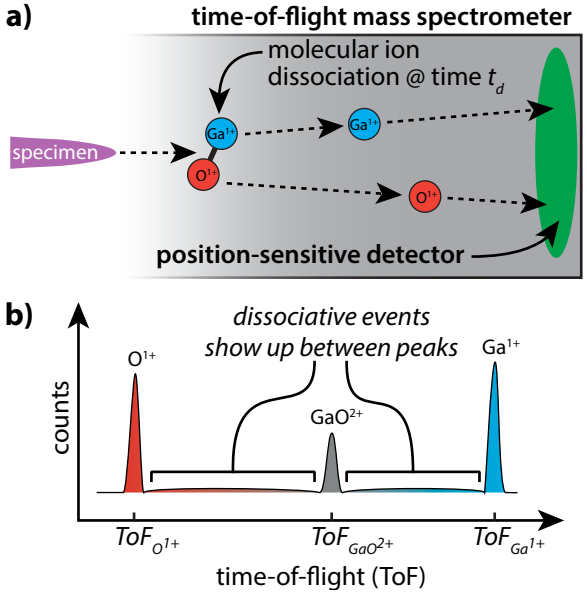

Figure 1: (a) Schematic of a dissociation event in an APT instrument. Here, a GaO^{2+} (parent) ion is extracted from the specimen tip and dissociates at a time t_d into Ga^{1+} and O^{1+} (daughter) ions. These daughter ions then continue in the flight tube until they strike the position sensitive detector – in this case a microchannel plate (MCP). (b) An illustration of what a mass spectrum corresponding to the GaO^{2+} dissociation event might look like to a crude approximation. Ions that dissociate between the specimen apex and the MCP will show up as a background feature between the parent and daughter ion peaks.

derivation assumes a constant m/z during the ion's flight. Early work showed that the m/z obtained for the daughter ions in these dissociation events will frequently appear in the background in the one-dimensional (1D) mass spectrum (Fig. 1b). Further analysis demonstrated that these daughter ions were not randomly distributed in the mass spectrum and, in fact, when plotted on a two-dimensional (2D) correlation histogram, the dissociation events form curved tracks due to the fact that the daughter ions are intrinsically temporally correlated.[5] Under the approximation of a near-instantaneous (or 'sudden') acceleration, equations were derived for the location of the dissociation track in the correlation histogram; these equations are parameterized by the fractional voltage drop experienced by the parent ion at the moment of dissociation.

The introduction of the correlation histogram as an APT analysis tool in conjunction with the derivation of the equations for dissociation tracks permitted the identification of numerous dissociation processes that are not obvious in the 1D mass spectra. The analysis of these dissociation tracks have permitted researchers to start asking/answering a variety of questions such as: How does ranging these dissociation events affect the observed composition?[5–7] Can the dissociation tracks associated with neutral daughter ions account for compositional biases?[6, 8–11] How do dissociation events affect spatial resolution?[8, 9, 12] What are the lifetimes of various molecular ions?[12–15] How does the electrostatic field affect molecular ion formation/dissociation?[10, 16–19] Which electronic states are dissociative?[10, 13, 16–18] How can dissociation events affect peak shapes in the 1D mass spectrum?[12, 20] How do these dissociation events show up for ToF mass analyzers utilizing different designs?[14, 20]

Herein we focus on the last of these questions. Specifically, we investigate how the ToF mass analyzer design affects how dissociation processes are observed in the 1D and 2D histograms. This is of particular importance given that many of the in-depth dissociation studies have been carried out using remote electrode atom probe instruments, while the most commonly used tools utilize local electrodes (LEs).[12, 14, 16, 18] We develop a 1D electrostatic model for four different ToF mass analyzer models utilizing both remote and local electrodes in addition to straight and reflectron flight paths. These models are then used to simulate the trajectory for a $GaO^{2+} \rightarrow Ga^{1+} + O^{1+}$ dissociation under various experimental parameters. Finally, data on Ga_2O_3 specimens was collected in both straight and reflectron based LE atom probe instruments and compared to the simulations. There was excellent agreement between the data and simulations which facilitates an understanding of several broad and previously unexplained features in the mass spectrum of Ga_2O_3.

2. Methods

2.1. Sample Preparation

The APT specimens in this manuscript were produced from two different β-Ga_2O_3 samples. One sample was unintentionally doped with Si during the growth process and one sample was intentionally doped with Si following the growth process. As measured by secondary ion mass spectrometry (SIMS), the unintentionally doped sample had a Si concentration of *ca.* $1.5 \times 10^{17}/cm^3$, while the intentionally doped sample had a Si concentration of *ca.* $3 \times 10^{19}/cm^3$ (data not shown). The atomic density of Ga_2O_3 is *ca.* $10^{23}/cm^3$ and so even in the intentionally doped Si sample the silicon peaks are only a minor component of the mass spectrum. For the purposes of this manuscript which focuses on the dissociation of GaO^{2+} these samples are treated as identical. A *ca.* 30 nm thick Ti layer was sputter-deposited on top of the samples to serve as a protective cap in addition to preventing charging in the ion/electron microscopes. Atom probe specimens were prepared via standard focused ion beam lift-out techniques onto silicon flat top coupons or transmission electron microscope (TEM) half-grids.[21]

2.2. APT Data Collection

The data included in this manuscript were collected following the parameters listed in Table 1. All data were collected on Cameca LEAP 4000 series instruments. Laser pulse energies (λ = 355 nm) in the neighborhood of 2 pJ

Table 1: Experimental parameters for atom probe datasets. See Fig. 2 for a description of the detector designs.

dataset	1	2	3
run ID	R44_03672	R44_04037	R31_21249
sample	Si-implanted	unintentially Si-doped	unintentially Si-doped
APT instrument	LEAP 4000X Si	LEAP 4000X Si	LEAP 4000X HR
ToF design	LE-BD	LE-BD	LE-Ref
pulse frequency	250 kHz	250 kHz	200 kHz - 250 kHz
flight length	90 mm	160 mm	nominally 382 mm
temperature	54 K	54 K	46 K
pulse energy	2 pJ	20 pJ	5 pJ
detection rate	0.3 %	0.3 %	0.3 %
# ions	21 M	7 M	22 M
multiples	46 %	50 %	44 %
V_S range	4.8 kV to 7.2 kV	3.5 kV to 7 kV	3.8 kV to 5.1 kV
figures	Fig. 9a-d, Fig. 10a-c, g, h	Fig. 10g, i	Fig. 11a, c-e

to 20 pJ were found to yield reasonably sharp peaks with a low risk of fracture. The effects of other run parameters (base temperature, detection rate, pulse frequency, etc.) were not explored. Nor was any possible compositional bias explored. No background subtraction was used. As will be discussed later, three experimental parameters were targeted for direct comparison with simulation: standing voltage, flight length (for the straight flight instruments), and flight path type (straight or reflectron).

2.3. Simulation

Very broadly, the ion trajectory simulations were performed in two steps.[22–24] First the ToF mass analyzer geometry was defined and a multiphysics package was used to solve for the spatially varying electrostatic fields. Second, these electrostatic fields were used to numerically solve for ion trajectories (including any molecular ion dissociation) from the specimen tip to the MCP surface. The results of the simulations (*i.e.* the observed ToF at which the ions strike the MCP) were stored for analysis and visualization.

2.3.1. Model Geometry and Electrostatics

The first step towards solving for the electrostatic field was to define the ToF mass analyzer model geometries; these are schematically shown in Fig. 2a-d (see the Supplementary Materials for more details). The three straight-flight models (Fig. 2a-c) and the first half-space of the reflectron model (Fig. 2d) are based on a common geometry. All models are contained within a 100 mm diameter grounded metal cylinder that mimics a vacuum chamber. All models have a metallic specimen tip (5° half-angle truncated with a 50 nm radius of curvature end-form unless otherwise noted) biased with the positive standing voltage (V_S) placed 90 mm (unless otherwise noted) from the MCP (or ion mirror in the case of the reflectron). For the ToF mass analyzer designs utilizing a LE, the LE was at ground potential and represented by a hollow truncated conical surface with a half angle of 45° and an opening diameter of 50 µm.

In the remote electrode (RE) model (Fig. 2a) there are no extra electrostatic elements to consider.[22] In the LE field-free drift tube (LE-FFD) model (Fig. 2b) a grounded LE is placed 50 µm in front of the specimen tip (unless otherwise noted) and an ≈ 60 mm diameter grounded flight tube encloses the path to the MCP. The LE biased drift tube (LE-BD) model (Fig. 2c) is identical to the LE-FFD model except that the MCP surface and flight tube are held at a fixed bias ($V_D = -3$ kV) that is independent of the standing voltage (V_S).[24]

In the LE field-free drift tube with reflectron (LE-Ref) model, the first portion of the ion's flight is identical to that of the LE-FFD model with a 90 mm flight length. However instead of an MCP, at the end of the flight tube is an electrostatic mirror consisting of a pair of parallel plate electrodes (the first one being a transparent mesh) parameterized by a separation (39 mm) and retarding potential ($V_R = 1.05 \times V_S$). After ions traverse the mirror, the remaining drift tube is assumed to have zero electrostatic field. The length of this final drift tube was 106 mm which satisfied the equation for time focusing.[23] In real reflectron-based mass analzyers (and for ease of visualization in Fig. 2d) the ion is deflected off axis (by an angle $< 180°$) however, for computational simplicity we choose to assume a perfect anti-parallel design. By assuming a perfect planar mirror (constant electrostatic field) and a field-free flight tube following the mirror, the ions can be propagated analytically in those two regions.

The model geometries are not intended to be exact replicas of any particular instrument, but are representative of different instrumental designs. The RE model is similar to the LaWaTAP.[12] The LE-BD model is a reasonable approximation to a LEAP 4000X Si[24] and the LE-Ref is a reasonable approximation to the LEAP 4000X HR. Both the LE-BD and LE-Ref models yield similar flight times as the LEAP 4000 series instruments.

The four model geometries shown in Fig. 2 (and the

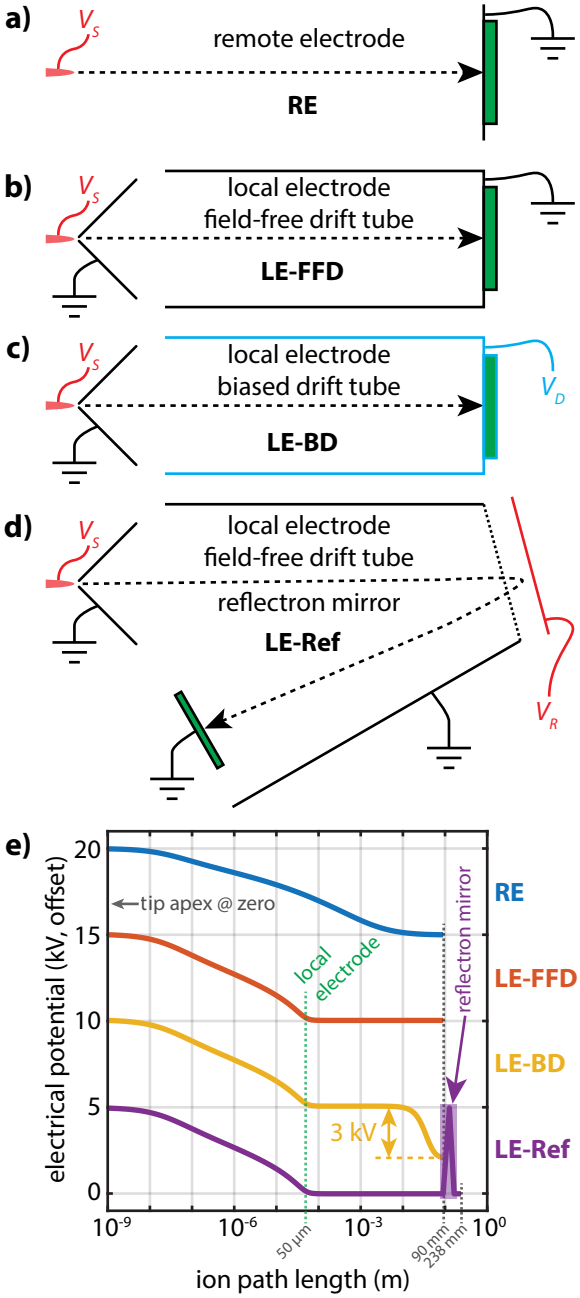

Figure 2: (a-d) Schematics of four different ToF mass analyzer designs. In all cases the specimen tip is held at $+V_S$. (a) Schematic of a ToF mass analyzer utilizing a remote electrode (RE) design. Here, the MCP serves as the counter electrode and is located far (90 mm) from the tip. (b) Schematic of a ToF mass analyzer utilizing a local electrode (LE) and field-free drift tube design (LE-FFD). Here, a grounded LE is placed in close proximity (50 µm) to the specimen tip. The flight tube and MCP surface are grounded. (c) Schematic of a ToF mass analyzer utilizing a LE and a negatively biased drift tube and MCP surface (LE-BD). (d) Schematic of a ToF mass analyzer utilizing a LE and a reflectron energy compensation ion mirror (LE-Ref). Here, after traversing the LE the ion is reflected by an electrostatic mirror back towards a MCP. (e) Plot of the electrostatic potential plotted as a function of ion path length for an *on-axis* ion trajectory ($V_S = +5$ kV). Regions with a flat electrostatic potential may be considered to be effectively field-free.

Supplementary Materials) were input in a multiphysics package (COMSOL 6.1) which was used to solve for the electrostatic fields. The field calculation is unique for each standing voltage, while in the experiments the voltage is continuously varied. Thus, to aid in direct comparisons between experiment and simulation, the simulations were performed in 250 V steps and averaged over the appropriate range of experimentally explored standing voltage. The electrostatic potentials obtained from the electrostatic calculations along the high symmetry axis of the ToF mass analyzer ($V_S = +5000$ V) are shown in Fig. 2e. For the mass analyzers utilizing a grounded LE, the electrostatic field emanating from the tip is screened by the LE which serves to anchor the electrostatic potential to ground potential in the vicinity of 100 µm from the specimen tip. In contrast, the electrostatic field is more spatially extended for the RE model since the only screening is by the chamber itself which results in a more slowly decaying electric potential. In the LE-BD model, the biased MCP/flight tube induces a weak electrostatic field at distances > 10 mm from the specimen tip. The LE-Ref model has an electrostatic mirror which means that an ion experiences a linearly increasing potential as it traverses (and eventually retraces) the mirror volume.

2.3.2. Ion Trajectory Simulations

For computational simplicity the ion trajectory simulations are 1D and only consider the electrostatic field and ion motion along the high symmetry axis. The ions were initially assumed to be at rest at the tip. The ions were propagated in the static electrostatic field using a Runge-Kutta based solver (`ODE45`, MATLAB 2022a). In the LE-Ref model, ions were propagated analytically in the electrostatic mirror and in the final field-free region.

For simulations including molecular ion dissociation events, the parent ion was numerically propagated until the prescribed dissociation time, t_d (or until the parent ion impacted the MCP surface). The dissociation time could either be explicitly defined or was drawn randomly from a exponential distribution with a characteristic decay parameter denoted τ_d. At this point in the trajectory, the parent ion was split into two daughter ions. The kinetic energy release (KER) associated with the dissociation event is known to be important in APT[12–14]. Here we take the energy difference between the (bound) GaO^{2+} minima and the infinitely separated Ga^{1+} and O^{1+} ions as an estimate of the KER which has been calculated using electronic structure theory to be 4.21 eV[25, 26]. The orientation of the molecular ion was assumed to be uniformly distributed on the sphere and so the simulations randomly select an orientation of the ion unless otherwise noted. The KER is small relative to the total kinetic energy of the ions and so for computational simplicity, the KER was allocated to the ions impulsively, assuming classical conservation of momentum – we note that more in-depth studies, especially three-dimensional models, would possibly need to revisit this assumption. Since this is a

1D model, the transverse components to the KER impulse were ignored. These daughter ions were then propagated until they intersected with either the MCP surface or, in the case of the LE-Ref model, if/when they intersect with the back electrode in the electrostatic mirror. The most important information from these trajectory simulations was the ion ToF, however the position and velocity of each ion as a function of time can also be extracted.

3. Results

3.1. Ion Trajectory Simulations

For each ToF mass analyzer model the electrostatic potential at the parent ion's location and the velocity of the parent ion are plotted as a function of time since leaving the tip (Fig. 3a-d); in this case no dissociation was simulated and the parent ions arrive at the MCP intact. The solid lines show the electrostatic potential and the dashed lines show the parent ion velocity – these lines terminate at the MCP surface at the observed parent ToF. The location of the entrance plane of the LE is noted, as is the period of time where the parent ion is inside the electrostatic mirror (for the LE-Ref model). For the RE model, the ion is accelerating continuously over the first *ca.* 10 ns (Fig. 3a). In contrast, the LE-FFD model has a grounded LE which concentrates the electrostatic field and forces the acceleration to occur within less than 1 ns (Fig. 3b). In the case of the LE-BD model, the ion experiences a second voltage drop close to the MCP surface that causes an additional acceleration (Fig. 3c). In the case of the LE-Ref model, the ion traverses the electrostatic mirror and reverses direction (Fig. 3d). What is important to keep in mind is that it is the electrostatic field (*i.e.* voltage gradient) that acts upon the ion(s) and changes the velocity and leads to the observed ToF. This, for example, is why the 'sudden approximation' equations derived for dissociation tracks given were able to be parameterized by the fractional voltage drop.[5]

As a first step towards understanding how dissociation events are observed in an experiment, the observed ToF is plotted for each mass analyzer model as a function of molecular ion dissociation time (Fig. 3e-h). These plots may be understood as follows. For infinitesimally small dissociation times the dissociation occurs while the ions are still at the tip surface and before any voltage drop has occurred. In this limit, the ToF of the daughter ions are indistinguishable from the direct correlated evaporation of the daughter ions directly from the tip surface (*i.e.* there never was a parent ion). In contrast, when the dissociation time is longer than the parent ion ToF the ion arrives intact and the single detected ion has the ToF of the parent ion. The present manuscript serves to connect these two limiting cases, *i.e.* what ToFs are observed for the daughter ions when $0 < t_d < ToF_{parent}$.

In the case of the RE model, the curves connecting the daughter ion ToFs to the parent ToF are continuous and relatively smooth in appearance. The daughter ion ToFs do not approach the parent ion ToF until close to *ca.* 100 ns.

In the case of the LE-FFD model, the daughter ion ToF curves approach the parent ion ToF within 1 ns of leaving the tip. This is consistent with the fact that the full voltage drop is localized between the tip and the LE meaning that once the parent ion passes through the electrode, the ion velocities are effectively unchanged regardless of whether or not dissociation occurs in the flight tube.

In the case of the LE-BD model, the daughter ion ToFs change continuously between the tip and the LE, and then they plateau at an intermediate value from about 1 ns to 100 ns before approaching the parent ToF value right before striking the MCP. Similar to the LE-FFD model, the voltage drop between the positively biased tip and the grounded LE occurs within 1 ns of the parent ion leaving the tip. Once through the LE opening, the electrostatic field is dramatically reduced and so the daughter ToFs plateau until the electrostatic field arising from the additional voltage bias between the LE and the MCP/flight tube acts upon the ions. Note, the first voltage drop (standing voltage) is varied during an APT experiment, while the second voltage drop is static.[24]

In the case of the LE-Ref model, things get a little more complicated due to the presence of the ion mirror. The first thing to note is that part of the ToF curve for the heavier Ga^{1+} daughter ion is missing (from $\approx 10^{-12}$ s to $\approx 10^{-6}$ s). This is because for a range of t_d, after the parent ion dissociates, the heavier Ga^{1+} ion has a kinetic energy significantly larger than the retarding potential on the ion mirror can reflect and so the ion strikes the back electrode of the ion mirror and is considered lost.[14] The maximum fraction of excess kinetic energy for a Ga^{1+} daughter ion is given by the ratio of the parent ion m/z to the daughter ion m/z, which in this case results in a Ga^{1+} daughter ion with up to 62 % excess kinetic energy relative to a Ga^{1+} emitted directly from the tip.[14] The retarding bias has a 5 % overpotential relative to the standing voltage ($V_R = 1.05 \times V_S$) and so it is clear that the Ga^{1+} ion may be lost for a range of t_d. A second feature apparent in the LE-Ref model is that, like the other models including a LE, there is a plateau in the ToF for the observed daughter ions (in this case the O^{1+} only since the Ga^{1+} is lost) once the ion passes through the LE. The daughter ToFs then approach the parent ToF as they traverse the ion mirror. Any dissociation that occurs in the field free flight tube following the ion mirror is difficult to directly observe because the two daughter ion ToFs would be identical (on average) to the parent ToF since there are no electrostatic fields to act on them.

One additional point to note from Fig. 3e-h is that the maximum effect of the KER and orientation of the molecular ion at the time of dissociation is shown as the shaded region around the solid lines. The edges of the shaded regions specifically define the two limiting orientations where the molecular ion axis is parallel and anti-parallel to the

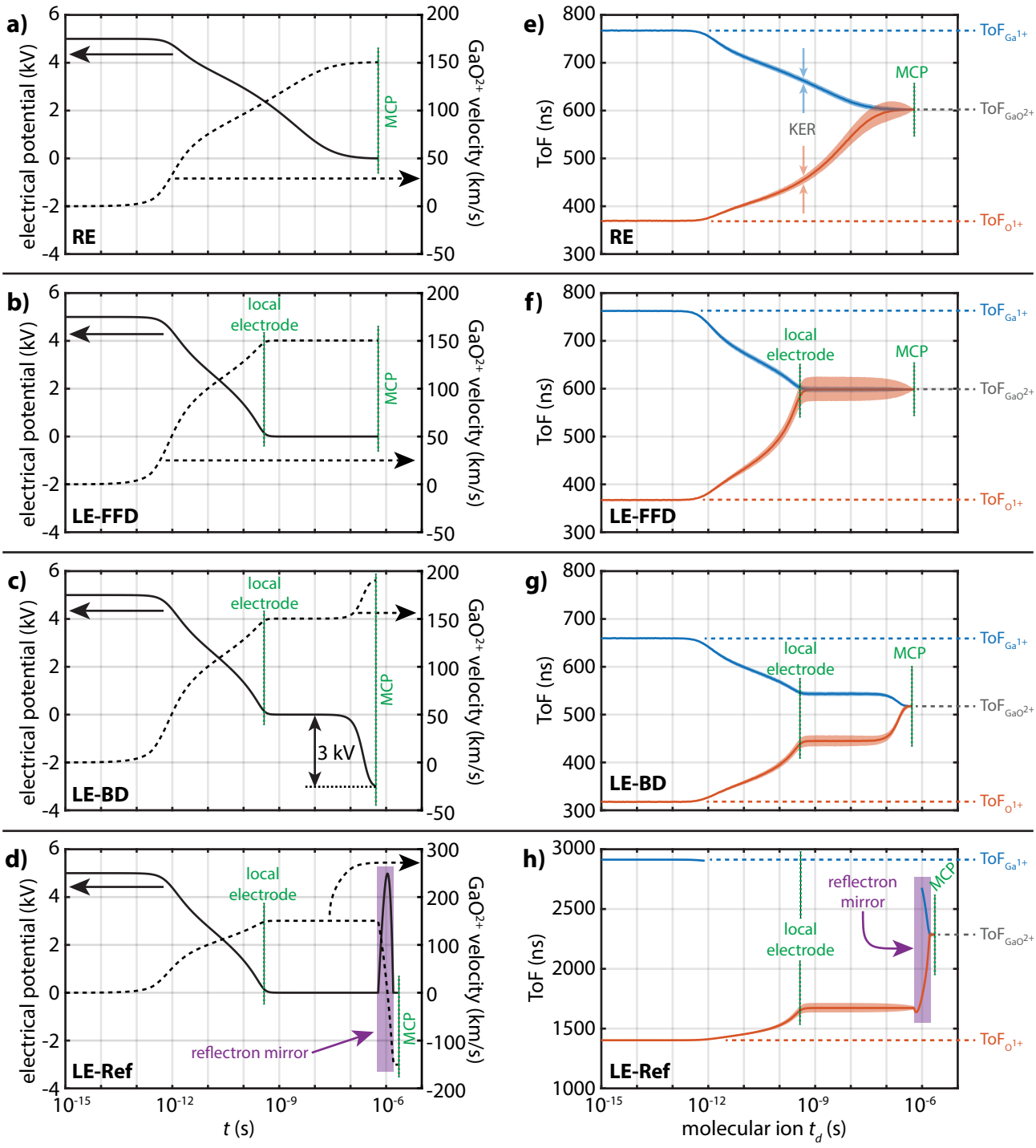

Figure 3: (a-d) Here we show simulated results from GaO^{2+} ion trajectories for each of the ToF mass analyzer designs. The solid line shows the electrostatic potential plotted versus time for the parent ion (note, this is the time associated with the ion trajectory and is not the ToF observed by the MCP, the ToF corresponds to when the trajectory terminates at the MCP). On the same time axis, the dashed line shows the parent ion velocity which emphasizes the effect of the electrostatic field on the ions. The approximate time when the ion traverses the LE is overlaid. The tracks end when the ion strikes the MCP. (e-h) Here we show simulated results from GaO^{2+} ion dissociation trajectories (parent and daughter ions) for each of the ToF mass analyzer designs. Very fast ($t_d < 10^{-12}$ s) dissociation events are indistinguishable from the direct evaporation of the two daughter ions. Very slow ($t_d \approx ToF_{GaO^{2+}}$) dissociation events are indistinguishable from the parent ion. In the simulation a coulomb-based kinetic energy release (KER) term is included that gives each ion an impulse radially out from the parent center of mass at the time of dissociation, which statistically modifies the daughter ToFs – this is plotted as the shaded region around each curve.

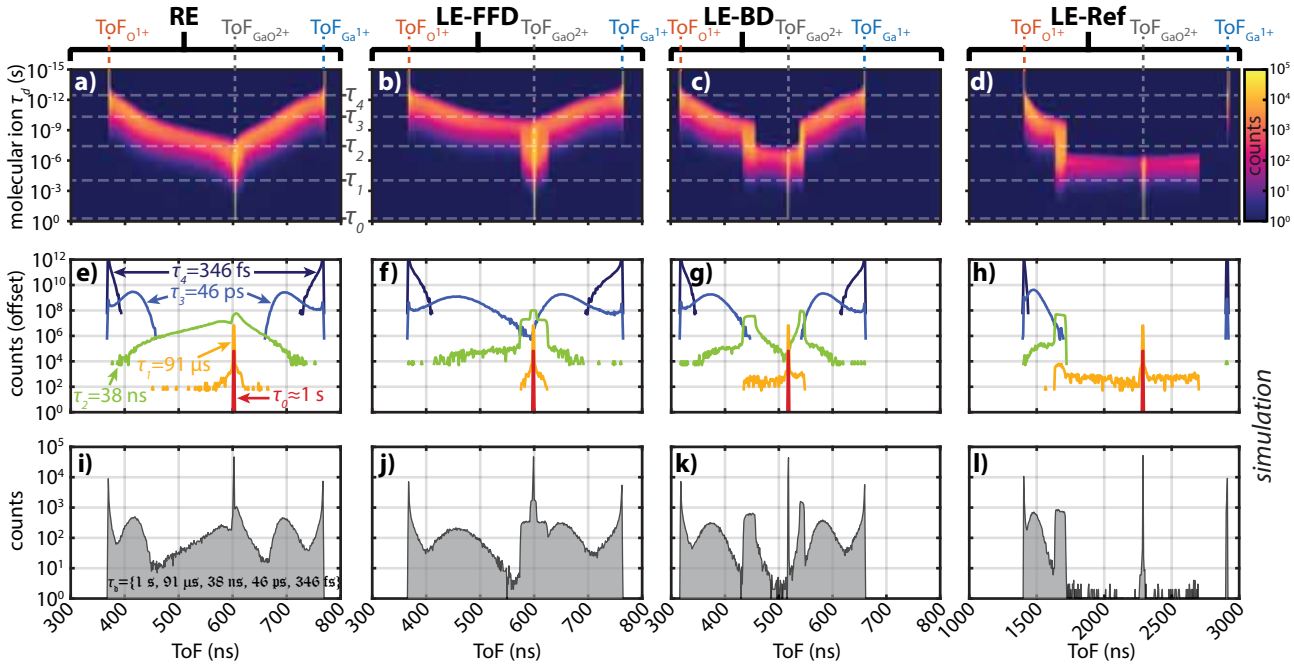

Figure 4: (a-d) Here we show simulated results from GaO^{2+} ion trajectories for each of the ToF mass analyzer designs. In contrast to Fig. 3 where the flight time was directly explored, these simulations are performed for exponential distributions of dissociation times, where τ_d is the distribution lifetime. This simulation more closely corresponds to the type of data that might be encountered in an experiment. Each horizontal cut through the heat map represents a simulated ToF spectra for a particular value of τ_d. Dashed lines are overlaid for the five theoretically predicted bound state lifetimes ($\tau_d = \tau_{n=0,1\ldots4}$). Thus, these graphs allows you to see how the parent ion lifetime affects the experimentally measured ToF spectrum. (e-h) The ToF mass spectra corresponding to five theoretically predicted lifetimes for the GaO^{2+} parent ion are shown. These correspond to the dashed lines in (a-d). (i-l) The sum of the spectra corresponding to the theoretical lifetimes are summed and plotted.

high symmetry axis of the flight path. It can be seen that depending on the exact design of the ToF mass analyzer the effect of the orientation and kinetic energy release can vary somewhat significantly. We should note here that this simulation is only 1D in nature and that fully 3D trajectory simulations would be necessary to understand the complete picture of how dissociation events affect APT reconstructions – *i.e.* the correlation between space and time in the trajectory aberrations due to dissociation.[12–14, 20, 27, 28]

While the data in Fig. 3 demonstrates the effect of the molecular dissociation time on the observed daughter ion flight times, it presents the data as a function of the dissociation time, which is not directly relevant to an experiment. In a real experiment, the dissociation time of molecular ions will be statistical in nature, arising from a distribution of initial quantum states and pathways.[10, 13, 16–18] A complete analysis of the kinetics of GaO^{2+} dissociation is well beyond the scope of the present study, however we can better connect the simulations to an experiment by assuming that the distribution of dissociation times is given by an exponential probability distribution. This may be regarded as the simplest physically reasonable assumption.

To this end, Fig. 4a-d shows 2D intensity plots of the ToF distributions generated for dissociation events for each mass analyzer; the sampled dissociation times (t_d) are drawn from an exponential distribution characterized by a lifetime of τ_d. In these 2D intensity plots, each horizontal line represents the ToF histogram that would be generated for a dissociation with a lifetime parameter of τ_d. The overall structure of these 2D intensity plots is quite similar to the ToF versus t_d plots in Fig. 3e-h (though the ToF axis is horizontal instead of vertical), except that the deterministic t_d value is replaced with the distributional τ_d parameter which results in a more realistic simulation.

In order to understand these simulations in the context of GaO^{2+} we need to consider the electronic structure of the parent ion. The parent ion is metastable (*i.e.* not thermodynamically stable and can dissociate via tunneling) such that each of the five theoretically predicted metastable vibrational levels have a distinct dissociation lifetime ($\tau_d = \tau_{n=0,1\ldots4}$).[26] The ToF histogram for each of the theoretically predicted lifetimes can be extracted as slices from the 2D intensity plots and are shown in Fig. 4e-h. For very short lifetimes ($\tau_4 = 346$ fs) the ToF histogram is peaked at where the Ga^{1+} and O^{1+} ions are expected, though 'tails' towards the parent peak are also present. In this case, the dissociation is occurring very close to the tip surface. For a slightly longer lifetime ($\tau_3 = 46$ ps) the peaks broaden significantly and move towards the parent ion peak. The broadness of the peaks is due to the rapid change in the electrostatic field that occurs in the vicinity of the tip. For an intermediate lifetime ($\tau_2 = 38$ ns)

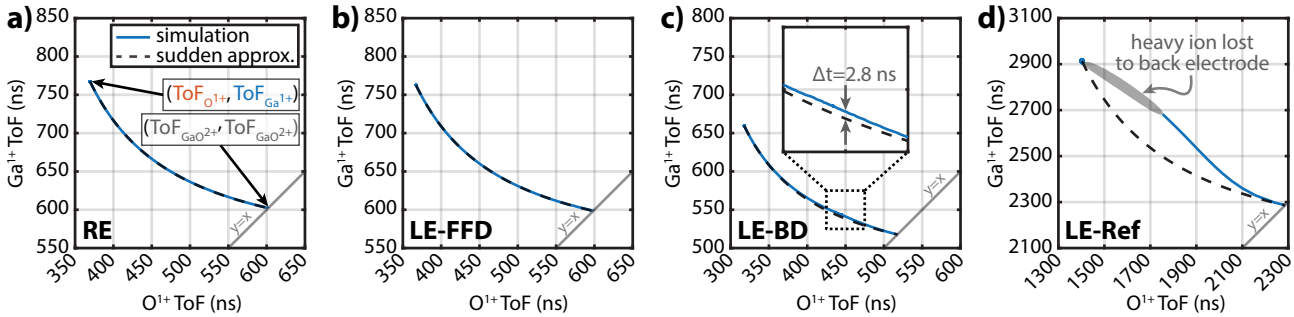

Figure 5: Simulations of the dissociation track paths (neglecting the kinetic energy release) for each of the ToF mass analyzer designs. Overlaid in dashed lines are the predictions of the sudden approximation discussed in Ref. [5]. Here, the bottom right end point corresponds to the parent ion ToF located on the line $y = x$ and the top left end point corresponds to the daughter ion ToFs. (a,b) For both the RE and LE-FFD designs the sudden approximation is indistinguishable on the plots. (c) For the LE-BD design the electrostatic field present near the MCP surface causes the simulated results to deviate measurably from the sudden approximation. (d) For the LE-Ref design, the presence of an electrostatic mirror in the middle of the flight path causes severe deviations from the sudden approximation. In this case, there is a large portion of the correlation track that is lost because the heavy (Ga^{1+}) ions strike the back electrode in the mirror and are not detected.

the different mass analyzers evidence quite distinct ToF histograms. In the case of the RE model, the continuous decay of the field gives rise to an exceptionally broad ToF distribution. In contrast, the addition of a LE means that, on average, the ions do not dissociate until after they pass through the LE aperture. Once through the LE aperture the electrostatic field is significantly smaller in magnitude and dissociation over a wide range of t_d results in only small difference in the observed ToFs. The resulting ToF histograms have a more rectangular or 'flat-top' appearance where the width is largely governed by the KER of the dissociation. For very long lifetimes ($\tau_1 \approx 91$ µs and $\tau_0 \approx 1$ s) the ToF histogram is nearly indistinguishable from that of the parent ion.

While there are literature values for the lifetimes of the metastable vibrational states of GaO^{2+}, the relative population of these states during/following field ionization is unknown. Thus, in order to compute a simulated ToF histogram for GaO^{2+} we must make an additional assumption. To get a general sense for what features may be present in a real histogram we choose to take an equal superposition of the five metastable vibrational states and plot the result in Fig. 4i-l. Within the constraints of the assumptions outlined above, these data can be taken as a simple model that should show the types of structures that may arise in the ToF histograms as a result of the dissociation of GaO^{2+}. Unless otherwise noted, the rest of the simulations in this manuscript utilize this population and lifetime model.

In an ideal instrument, the technical details of the chosen mass analyzer would play only a minor role in determining the structure of the resulting histogram. *However, here we find that the simulated histograms depend somewhat strongly on the ToF mass analyzer geometry.* In the case of the RE model, the space between the parent and daughter peaks is dominated by broad features. In the LE-FFD model, the features are even broader and the parent peak has a square pedestal. In the LE-BD model, the broad features are still present, but there are additional flat-top features that have appeared. And in the case of the LE-Ref model, the broad feature and the flat-top feature are present near the O^{1+} ion peak, but there are no corresponding features near the Ga^{1+} peak. Each of these structures can be understood with the help of Fig. 3e-h and Fig. 4a-d . For example, the broad features close to the Ga^{1+} and O^{1+} peaks are associated with the decay of the electrostatic field between the tip and the electrode (remote or local). The square pedestal of the LE-FFD parent peak and the extra flat-top features in the LE-BD model and LE-Ref models are due to the KER for a dissociation that occurs after the parent ion has passed through the LE and into a region where the electrostatic field is relatively weak.

The previous discussion focused on the appearance of dissociation events in the 1D ToF histogram. However, as noted previously, daughter ions are intrinsically correlated in time and so it is worthwhile trying to understand how that time correlation is observed. Fig. 5 shows the correlation from the trajectory simulations between the O^{1+} ToF and the Ga^{1+} ToF as a solid line for each ToF mass analyzer as the dissociation time is varied from zero to infinitely long. In the case where $t_d \approx \infty$ the curves terminate along the line $y = x$ at the GaO^{2+} ToF. In the case where $t_d = 0$ the curves terminate at the point corresponding to the ToF for the two daughter ions. Overlaid on each plot as a dashed line is the widely used parameterization (we denote it as the 'sudden approximation') that assumes that the ion acceleration entirely occurs very close to the tip (see Ref. [5] for details). Note that for clarity, these plots do not include KER.

Visual inspection of Fig. 5 dissociation tracks reveal that the sudden approximation is not obviously distinguishable from the trajectory simulation for the RE and LE-FFD models. In the case of the LE-BD model, the sudden approximation deviates by several nanoseconds due to the presence of an electrostatic field in the flight tube far

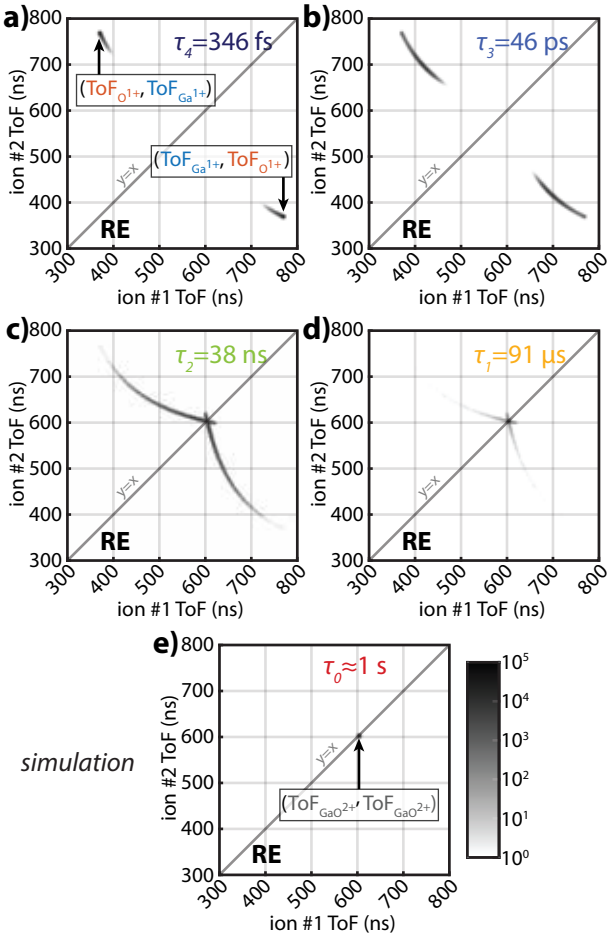

Figure 6: Simulations of the correlation histogram for a GaO^{2+} dissociation event for the theoretically predicted lifetimes for the RE model. (a) For very short ion lifetimes the ions tend to dissociate in close proximity to the tip apex before a significant traversal of the total voltage drop has occurred. These events appear as the correlated evaporation of two daughter ions. (b-d) As the lifetime lengthens, the ions dissociate at intermediate times and yield flight times that correspond neither to the parent ion nor the daughter ions. (e) For long ion lifetimes the ions tend not to dissociate at all before striking the MCP and are registered as a parent ion.

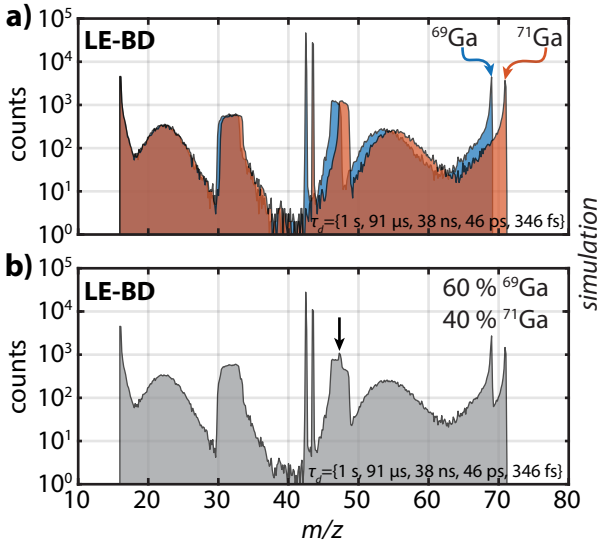

Figure 7: (a) Simulations on the effect of the Ga isotopes on the 1D m/z spectrum. Two mass spectra are shown – one for each of the main Ga isotopes. (b) Here the weighted sum of the two Ga isotope spectra is plotted. Notably, the overlap between the flat-top features around 47 m/z result in a sharp feature on top of a pedestal indicated with an arrow. The prediction of this feature can be compared to experiment as a test of the veracity of the model.

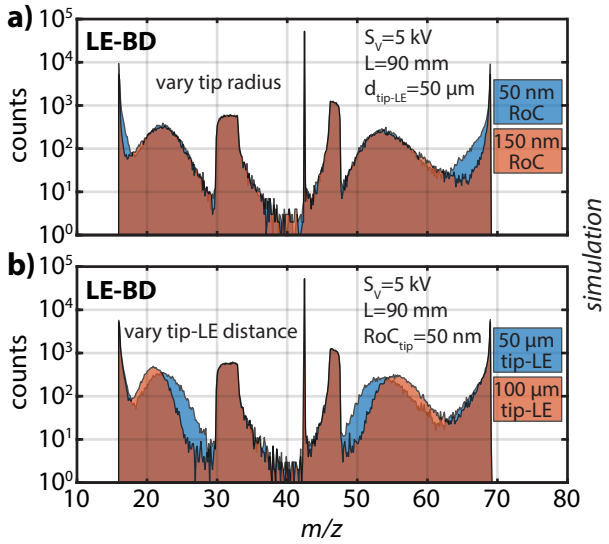

Figure 8: (a) Simulations on the effect of the tip radius of curvature (RoC) on the simulated spectrum. The tip RoC changes the electrostatic field at the tip and primarily affects the tails of the daughter peaks. (b) Simulations on the effect of the distance between the specimen apex and the LE on the simulated spectrum. The tip-LE separation primarily affects the dynamics of the ions in the time range of 10^{-12} s to 10^{-9} s and affects the broad features in the mass spectrum.

from the tip. In the case of the LE-Ref mode, as might be expected due to the presence of the ion mirror in the middle of the ion flight time, the assumptions of the sudden approximation are entirely inappropriate and so the deviation between the sudden approximation and the trajectory simulations is large. In addition, a section of the dissociation track is absent due to the loss of the heavier Ga^{1+} ion to the back electrode. Important to note is that because the dissociation track requires a correlation between the two daughter ions, the loss of the Ga^{1+} ion means that the O^{1+} ion is also missing from the dissociation track. These data suggest that the sudden approximation may have limitations as a tool for the quantitative analysis of dissociation track data depending on what type of mass analyzer is being used on an instrument. Given that most instruments in use resemble LE-BD or LE-Ref, these data suggest that using the sudden approximation equations to extrapolate the identity of a parent ion or daughter ions may result in non-trivial mass errors especially when only small portions of the dissociation track are visible.

The results presented in Fig. 4 and Fig. 5 can be visualized together by simulating a 2D correlation histogram

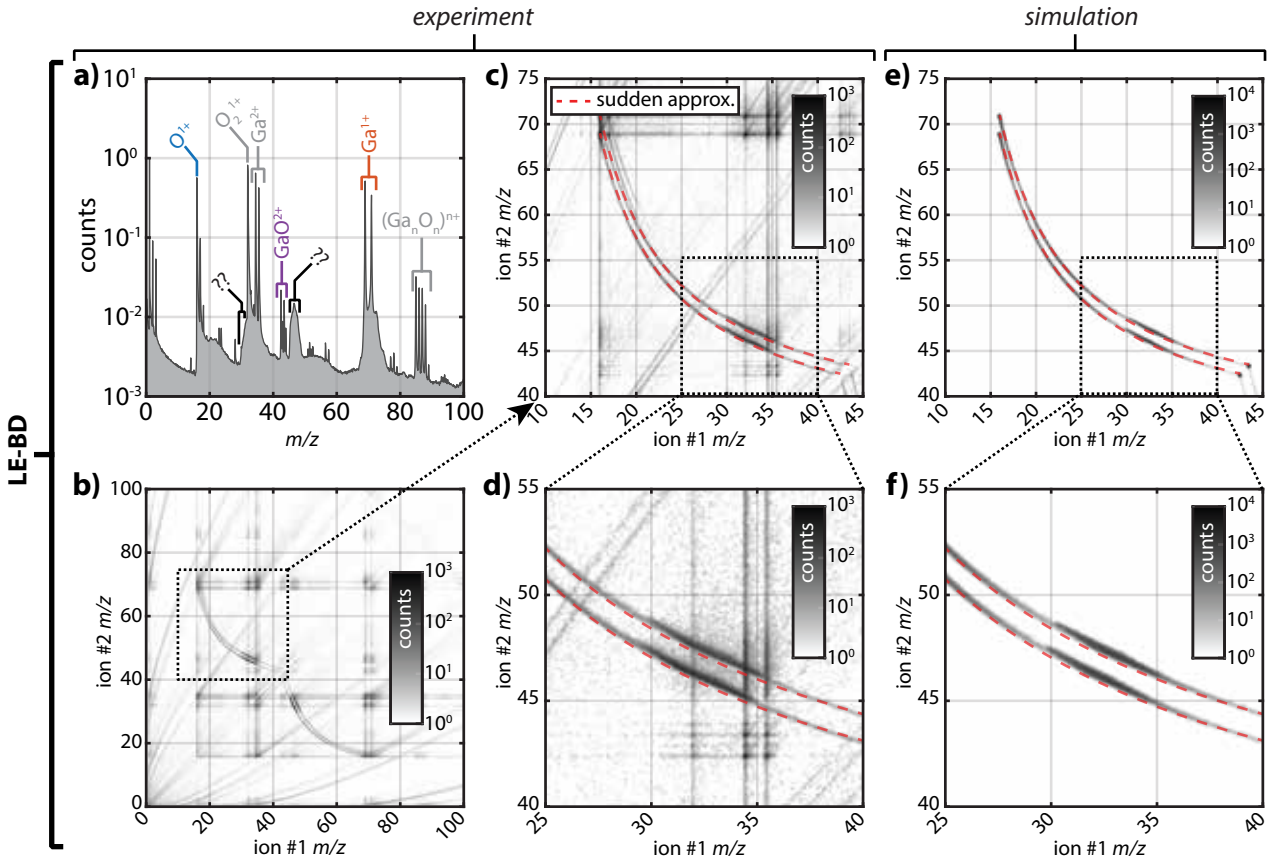

Figure 9: A comparison of simulation and experiment for a LE-BD (*i.e.* LEAP 4000X Si) ToF mass analyzer configuration. (a) Experimental mass spectrum collected for a Ga_2O_3 tip with the relevant peaks labeled. The features denoted with question marks (??) are caused by the ion dissociation process. (b-d) An experimental correlation histogram showing the $GaO^{2+} \rightarrow Ga^{1+} + O^{1+}$ dissociation track at increasing magnifications. Overlaid is the expected dissociation track from the sudden approximation. (e-f) Simulated correlation histogram data corresponding to the experimental shown in (c-d).

(presented here for the RE model). The correlation histograms for the dissociation lifetimes theoretically predicted for GaO^{2+} are shown in Fig. 6. Here we can see how the correlation in the distribution of measured ToFs evolves as the dissociation lifetime changes. We have symmetrized the histogram across the line $y = x$ to better match what would be observed in an analysis of experimental data. For short lifetimes the intensity in the tracks is localized near the daughter ion ToFs, and this intensity moves towards the parent ToF as the decay lifetime increases. Similar plots can be made for the other ToF mass analyzers, however these are omitted since they do not yield insights that are not already apparent from Fig. 4 and Fig. 5.

Before comparing the trajectory simulations to experimental data it is worth investigating how certain experimental realities might affect these simulation results. First we consider the isotopic distribution for GaO^{2+}. For the purposes of this work, oxygen can be regarded as monoisotopic (> 99% ^{16}O), however gallium has two stable isotopes in comparable abundances: 60 % ^{69}Ga and 40 % ^{71}Ga. Including these two Ga isotopes into simulations can lead to somewhat unexpected results. Fig. 7a shows the individual 1D m/z histogram for $^{69}Ga^{16}O^{2+}$ and $^{71}Ga^{16}O^{2+}$ in the correct abundance plotted for the LE-BD model. Fig. 7b shows the sum of these histograms which is close to what would be expected experimentally. As expected, the Ga^{1+} and parent peaks split while there is only one O^{1+} peak. The sum of the flat-top features between the parent and Ga^{1+} peaks results in a sharp feature on a flat-top pedestal indicated by an arrow in the figure.

Next we consider the tip shape and its distance from the LE in the LE-BD model as these can vary during and/or between nominally identical APT experiments. In Fig. 8a the tip radius of curvature (RoC) was varied from 50 nm to 150 nm and the m/z histograms are shown. At a constant standing voltage, the changing tip RoC changes the electrostatic field in the vicinity of the tip surface and so this predominately affects the dissociation events that occur near the tip surface and thus affects the histogram in the vicinity of the daughter peaks. In Fig. 8b the spacing between the LE and the tip was varied from 50 µm to 100 µm and the m/z histograms are shown. Here we see the main change in the histograms occurs as a shift in the broad features. This is consistent with the understanding

that the broad features arise from dissociations occurring between the tip and the LE in the first nanosecond or so of the parent ion's flight time. Taken together, Fig. 8a and Fig. 8b suggest that differences in the tip position (relative to the LE) and changes in the tip shape can affect the m/z histogram in minor ways and small changes in the observed line shapes should be interpreted with care.

3.2. Comparison to Experiment

3.2.1. LE-BD Model (LEAP 4000X Si)

The majority of APT instruments currently in use are commercially available systems that use LE designs. Herein we compare the GaO^{2+} dissociation trajectory simulations to data collected from Ga_2O_3 samples on two different APT instruments utilizing different ToF mass analyzer designs. The first instrument is a LEAP 4000X Si which served as the basis for the LE-BD model. The second instrument is a LEAP 4000X HR which served as the basis for the LE-Ref model.

A normalized m/z histogram from the LEAP 4000X Si instrument for a typical dataset is shown in Fig. 9a. The peaks relevant to the GaO^{2+} dissociation are labeled. In addition, two notable broad features are indicated with '??' around 33 m/z and 47 m/z. Inspection of the 2D correlation histogram (Fig. 9b-d) from the data reveals that these features arise from a localization of intensity on the GaO^{2+} dissociation track. Dissociation trajectory simulations utilizing the experimental standing voltage and flight length are presented in Fig. 9e-f for comparison. Additionally, the sudden approximation for the dissociation tracks is overlaid for comparison. The agreement between the simulation and experiment is striking, especially when we consider that no parameters were adjusted to obtain agreement. The localization of intensity in the correlation histogram (Fig. 9d,f) has the same origin as the flat-top features noted previously in the simulated 1D histograms and the features indicated with '??' in the experimental 1D histograms.

More detailed comparisons between simulation and experiment where the standing voltage and flight path length were varied are presented in Fig. 10. As the simulations only account for the dissociation process and not the multitude of other peaks in the mass spectrum, a comparison to experiment must isolate the dissociation process. Thus, 1D m/z histograms are shown (Fig. 10a,g) where only events within 1 m/z of the correlation track in the 2D correlation histogram are counted. This method is not perfect however, and so some features remain in these data that arise from other species (for example, the two sharp peaks around 35 m/z are from Ga^{2+}).

Fig. 10a-c shows the effect of standing voltage on the experimental data. The two features around 33 m/z and 48 m/z (indicated as '??' in the 1D experimental histogram) shift toward the parent ion peak as the standing voltage is increased. These shifts in the 1D m/z histogram can also be seen in the 2D correlation histogram as a shift in the distribution of counts along the dissociation track. The corresponding simulation data is shown in Fig. 10d-f and exhibits the same behavior. Note that the lineshape associated with the feature around 48 m/z (sharp peak on a pedestal) matches qualitatively with the expectation for the Ga isotopes seen in Fig. 7.

Fig. 10d-f shows the effect of flight length on the experimental data. The two features around 33 m/z and 48 m/z (indicated as '??' in the 1D experimental histogram) shift away from the parent ion peak as the flight length is increased. These shifts in the 1D m/z histogram can also be seen in the 2D correlation histogram as a shift in the distribution of counts along the dissociation track. The corresponding simulation data is shown in Fig. 10j-l and exhibits the same behavior.

3.2.2. LE-Ref Model (LEAP 4000X HR)

A normalized m/z histogram from the LEAP 4000X HR instrument for a typical dataset is shown in Fig. 11a. The peaks relevant to the GaO^{2+} dissociation are labeled. In addition, one notable broad feature is indicated with '??' around 25 m/z. In contrast to the data collected on the LEAP 4000X Si instrument, inspection of the 2D correlation histogram (Fig. 11c-e) does not give any direct clue as to the origin of the broad feature. However, 1D m/z histograms generated from dissociation trajectory simulations utilizing the experimental standing voltage and flight length are presented in Fig. 11b for comparison. Here the feature is reproduced well and corresponds to O^{1+} ions that derive from GaO^{2+} ions that dissociate between the LE and the ion mirror. For the dissociation events that correspond to this feature, the Ga^{1+} is lost to the back electrode and thus this part of the dissociation track is lost. In contrast to the LEAP 4000X Si data, the change in the standing voltage does not cause the feature at 25 m/z to shift notably, instead only the width changes slightly.

Next we can compare the experimental 2D correlation plot to the simulated 2D correlation plot in more detail. The experimental 2D correlation histograms are given in Fig. 11c-e and the simulated 2D correlation histograms are given in Fig. 11f-h. Given that, for many of the dissociation events, the Ga^{1+} ion is lost, a simulated 2D correlation plot will necessarily have no memory of these Ga^{1+} ions. To simulate something closer to an actual experiment, for dissociation events where the Ga^{1+} ion is lost, we draw a random m/z value using the 1D m/z histogram as the probability distribution; the result of this procedure is shown in Fig. 11f. Comparing 11c to Fig. 11f it can be seen that the loss of Ga^{1+} manifests as orthogonal overlapping 'bands' of counts in the 2D correlation histogram evident in the circled region of the correlation histogram. Zooming in on the GaO^{2+} dissociation track (Fig. 11d,g) we can see agreement between experiment and simulation for the strong difference between the actual dissociation track (indicated with arrows) and the track generated using the sudden approximation. Finally, zooming in further on the parent ion location (Fig. 11d,g) we can see how the

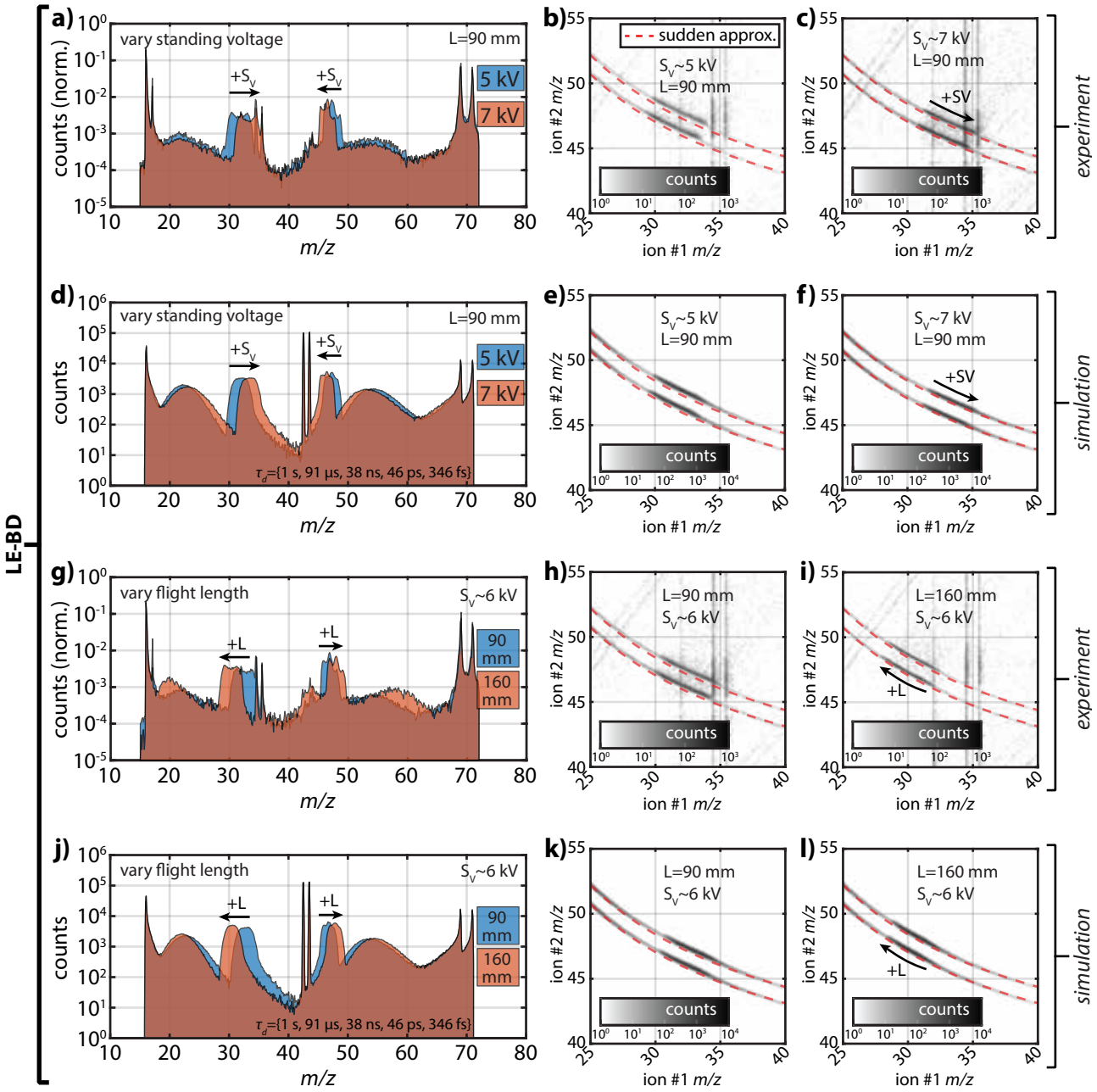

Figure 10: A systematic comparison of simulation and experiment for a LE-BD (*i.e.* LEAP 4000X Si) ToF mass analyzer configuration. Labels on the right-hand side of the figure identify which plots are experimental and which are from simulation. (a) The mass spectrum extracted from the vicinity of the dissociation track in a correlation histogram for two different standing voltages. An increase in the standing voltage has the effect of moving the large features towards the parent peak. (b-c) Correlation histograms for the same two standing voltages showing that the intensity along the track moves towards the parent as the standing voltage is increased. (d-f) Simulated data corresponding to the experimental data shown in (a-c). (g) The mass spectrum extracted from the vicinity of the dissociation track in a correlation histogram for two different flight lengths. An increase in the flight length has the effect of moving the large features towards the daughter peaks. (h-i) Correlation histograms for the same two flight lengths showing that the intensity along the track moves towards the daughter peaks as the flight length is increased. (j-l) Simulated data corresponding to the experimental data shown in (g-i).

kinetic energy release imparts a cross-like structure to that region of the dissociation track. The ions forming these crosses originate from dissociation events that take place following the ion mirror where the orientation of the ion at the time of dissociation either speeds up or slows down the ions in an anticorrelated manner.[12, 14]

4. Discussion

Although not the focus of this manuscript, it is worth starting the discussion by mentioning that the original reason our laboratory obtained Ga_2O_3 samples was to investigate the spatial arrangement of Si dopants. To this end, we needed to quantify Si peaks in the mass spectrum. As

can be readily seen in Fig. 10, for a LEAP 4000X Si instrument there is a flat-top feature indicated with '??' associated with Ga^{1+} daughter ions derived from the GaO^{2+} parent ion that may overlap with the Si^{1+} peak at 28 m/z depending on the standing voltage and flight length. This feature was significant enough to render the quantification of the 28 m/z peak difficult and at the time we had no understanding of the origin of this signal.

A literature survey of APT studies on Ga_2O_3-based materials showed a few interesting things. First, broad unexplained features have been commonly observed in studies of Ga_2O_3. A study using a LEAP 4000X Si instrument observed unassigned and unexplained features in the vicinity of 33 m/z and 48 m/z that match well with our observations (see Fig. S8 in Ref. [29]). A study using a LEAP 4000X HR instrument observed a broad feature around 23 m/z (personal communication, Ref. [30]). A separate study using a LEAP 5000XR also observed a broad unassigned feature around 23 m/z (see Fig. 12 in Ref. [31]). Finally, a study using a LaWaTAP (remote electrode based ToF mass analyzer) observed very broad features in the baseline centered in the vicinity of 25 m/z and 55 m/z.[15] These authors make no definitive assignment but discuss the possibility that these 'humps' are due

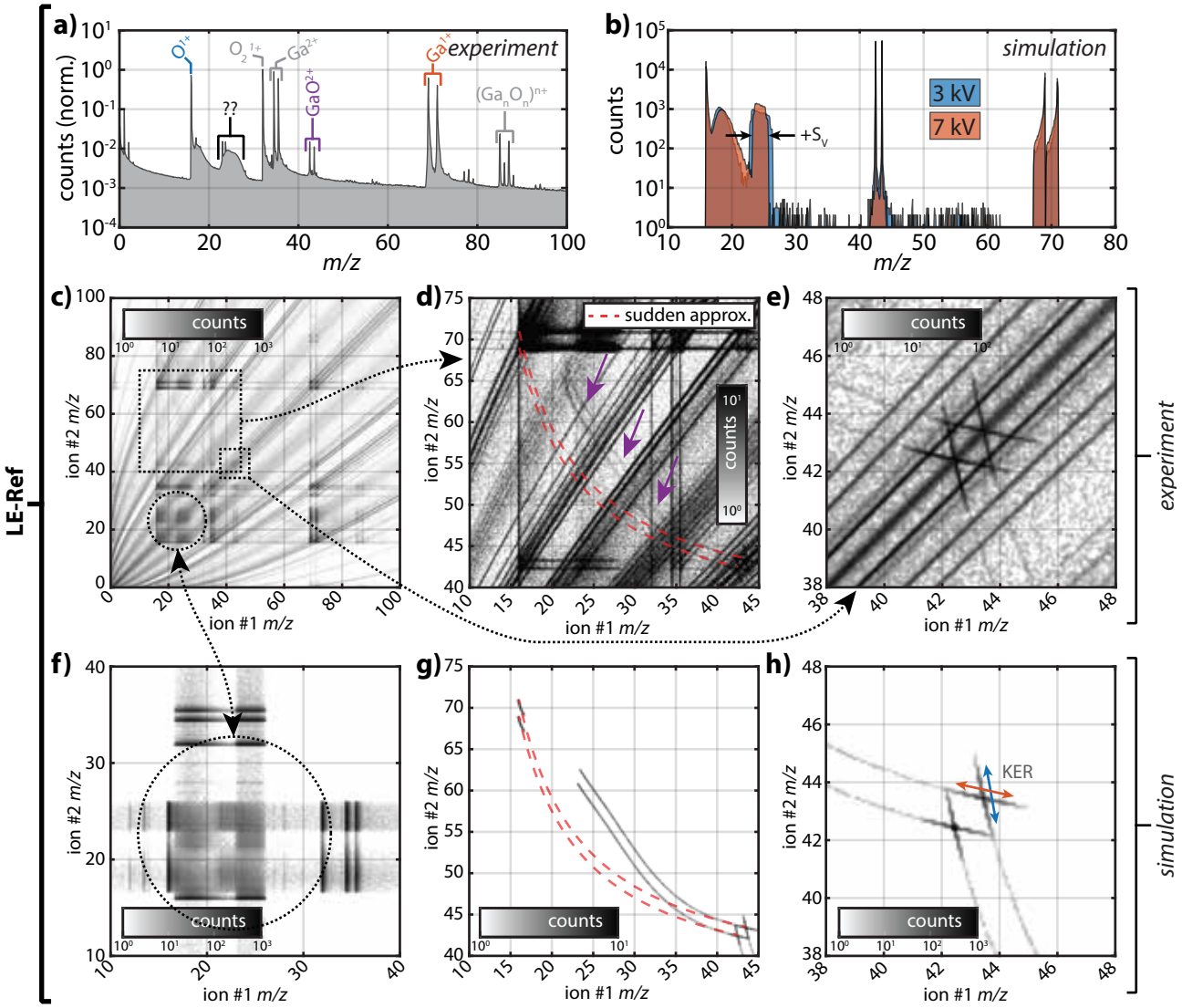

Figure 11: A comparison of simulation and experiment for a LE-Ref (*i.e.* LEAP 4000X HR) ToF mass analyzer configuration. (a) Experimental mass spectrum collected for a Ga_2O_3 tip with the relevant peaks labeled. The feature denoted with question marks (??) is caused by the ion dissociation process. (b) Simulated mass spectra showing the relatively minor impact of the standing voltage on the noted feature – instead of changing position it just changes width slightly. (c-e) An experimental correlation histogram showing the $GaO^{2+} \rightarrow Ga^{1+} + O^{1+}$ dissociation track at increasing magnifications. The dissociation track is faint and is indicated in (d) with arrows. Overlaid in (d) is the expected dissociation track from the sudden approximation. (f) A simulated correlation histogram that roughly accounts for the effect of the Ga^{1+} ions that were lost in the reflectron. Specifically, each lost Ga^{1+} is replaced with an ion randomly generated using a probability distribution given by the experimentally obtained 1D mass spectrum – this leads to the banding that is observed experimentally in (c) in the circled region. (g,h) Simulated correlation histogram data corresponding to the experimental data shown in (d,e).

to the delayed evaporation of cluster ions. Generally, the literature has observed that the mass spectrum produced from Ga_2O_3 during APT analysis has broad features and only one study suggested a possible cause. This is an unsatisfactory situation especially since as can be seen from Fig. 9a and Fig. 11a, the peaks marked with '??' are quite significant and can contain up to *ca.* 1/3 as many counts as are in the 16 m/z O^{1+} peak.

The simulations and experiments presented herein definitively assign these features in the mass spectra of Ga_2O_3 as resulting from the dissociation of $GaO^{2+} \rightarrow Ga^{1+} + O^{1+}$. The fact that the signature of a dissociative process is so prominent in the 1D mass spectrum appears to be somewhat uncommon. Or phrased differently, many materials show clear dissociation tracks in the correlation histogram, but do not show a prominent signature of these dissociations tracks in the 1D mass spectrum. One likely reason that Ga_2O_3 shows prominent molecular dissociation signatures in the 1D mass spectrum is that the parent ion may be emitted with significant probability in a quantum state that has a lifetime in the range of 100 ps $< \tau_d <$ 100 ns. For this range of lifetimes, the dissociation, on average, occurs far from the tip and far from the detector. As such, we emphasize that these dissociations are not field induced, but are intrinsic to the parent ion. We speculate that for most materials studied in APT, the probability of populating a particular quantum state during field ionization with a lifetime in this range is generally low. Our logic is as follows. For very small barrier heights, the strong electrostatic field has the capacity to assist in dissociating the ion in the vicinity of the tip. For barrier heights much greater than the thermal energy of the system, the probability that states are populated that have a lifetime shorter than the parent ToF is quite small. And so there is probably a narrow range of barrier heights for which these features can be observed in the 1D mass histogram with high probability. In most samples studied in APT, the correlation histogram is very sensitive to dissociation processes, so many dissociation tracks apparent in a correlation histogram may have little impact on the 1D m/z histogram.

Of particular importance in this work is the conclusion that different ToF mass analyzer designs can give rise to strongly differing signatures for the same dissociation process. This arises because a dissociation event intrinsically violates the assumptions of all ToF mass analyzers by dissociating after leaving the specimen tip and, as such, the observed ToF is strongly dependent on the exact electrostatic design of the detector (as is detailed in Fig. 3e-h). On one hand this fact is yet another cause for APT studies on the same material to differ, which makes the interpretation and comparison of data between groups more difficult. On the other hand, it suggests that certain instruments may be particularly sensitive probes of certain physics. For example, if the KER of a species with a > 1 ns lifetime is of interest, then an instrument with a LE-FFD could be used and the appearance of the anticorrelated cross-like feature at the location of the parent ion peak in the correlation histogram would encode the details of the KER process. Alternatively, if quantification of a particular low abundance element is desired, then the standing voltage and detector bias in a LE-BD instrument could be chosen to move features related to dissociative processes away from that region of the mass spectrum (effectively improving the sensitivity of the measurement).

We can also consider our results in terms of making peak assignments. In a correlation histogram, dissociation tracks are relatively straightforward to isolate and range.[6, 7] However, the imperfect detection efficiency of MCP-based detectors ensures that the dissociation track ions are mixed into the 1D mass histogram in significant proportions. For a detector with a hypothetical detection efficiency of $\eta = 0.5$, the probability that one of two ions is lost is given by $2\eta(1-\eta) = 0.5$, the probability that both ions are detected is given by $\eta^2 = 0.25$, and the probability that both ions are lost is given by $(1-\eta)^2 = 0.25$. Thus, the number of daughter ions visible in the correlation histogram (and the 1D mass histogram) is roughly the same as the number of daughter ions appearing in the 1D mass histogram (and not the correlation histogram). In a remote electrode instrument, the features due to dissociation in the flight tube are broad enough as to render them impractical to range in the 1D mass spectrum.[15] In an instrument with a LE-FFD design, the ranging of the parent peak would need to include the pedestal of the parent peak. While in a LE-BD instrument, the Ga^{1+} and O^{1+} daughter ion features associated with the flat-top features might be able to be ranged separately and included in a reconstruction. In contrast, in a LE-Ref instrument, only the O^{1+} feature is present and so this peak would need to be assigned to the parent ion to prevent undercounting the Ga^{1+} species. For most materials studied so far, quantifying dissociation tracks has not changed the overall composition significantly,[6–8, 11] but nonetheless ranging detected ions as correctly as possible is always desired.

Something that has been discussed previously in the literature, but worth emphasizing is that dissociation tracks are not easily parameterized by the identity of the parent ion and a single lifetime. Herein, we considered the vibrational quantum states of the ground electronic state potential energy surface which have lifetimes spanning many orders of magnitude, but even that is an oversimplification as excited electronic and rotational states, the spatially (and potentially time) varying surface field, and other factors also play an important role in determining how ions dissociate.[10, 13, 16–18] Attempts to extract lifetimes from dissociation tracks should therefore always be viewed as an order of magnitude estimate for the particular ensemble of quantum states being emitted from the tip during that APT experiment. Discussing the 'lifetime of a GaO^{2+} ion in an APT experiment' is incomplete and can be misleading without appropriate context.

Worth considering further is that the dissociation tracks derived under the sudden approximation differ measurably

from those simulated for a LEAP 4000X Si detector. Thus, for dissociation tracks that must be extrapolated to determine the identity of a parent ion, the sudden approximation may yield small errors. For example, a recent study on $FeO_3^{1+} \rightarrow O_2 + FeO^{1+}$ dissociation tracks on a LEAP 5000XS instrument noted that the parent ion that was extrapolated using the sudden approximation dissociation track parameterization yielded a parent ion that was about 2 m/z heavier than expected.[32] They postulated that the extra 2 m/z was due to H atoms, but further noted that the addition of two H atoms rendered the reaction energetically unfavorable as calculated from density functional theory. Given the simulations on the LE-BD (based on the LEAP 4000X Si) for GaO^{2+}, it seems at least somewhat probable that a dissociation track accounting for the actual electrostatics of the LEAP 5000XS ToF mass analyzer would not require the addition of two H atoms. In a similar vein, a close inspection of the dissociation tracks for GaN^{2+} in the paper that first derived the sudden approximation evidences a similar discrepancy between the sudden approximation for the dissociation track and the experimental data.[5] In general, the larger the difference in m/z between the parent and the daughter ions, the larger the deviation will be.

5. Conclusions

Herein we simulated the trajectories for parent and daughter ions of the $GaO^{2+} \rightarrow Ga^{1+} + O^{1+}$ dissociation process using four different ToF mass analyzer models including those commonly found on commercially available APT instruments. Each analyzer produces a spatially distinct arrangement of electrostatic fields which strongly influences how these daughter ions appear in the collected 1D and 2D histograms. We demonstrate by comparison between experiment and simulation that the broad unassigned features in the published APT m/z histograms of Ga_2O_3 arise from these daughter ions. Simulated dissociation tracks are compared to the 'sudden approximation' dissociation tracks commonly employed in the analysis of APT correlation histograms and the differences are discussed. Broadly, this work emphasizes that for events where the basic time-of-flight analyzer assumptions are violated, the specific design/electrostatics of a detector has a strong impact on how those events appear in the observed data.

Acknowledgments

We gratefully acknowledge financial support from the NIST Innovations in Measurement Science (IMS) program. In addition we thank David Diercks and Ty Prosa for helpful discussions. We thank Rebecca L. Peterson and Ming-Hsun Lee from the University of Michigan for graciously providing the Ga_2O_3 samples. DKS and KHY acknowledge funding from the U.S. Department of Energy (DOE), Office of Science, Basic Energy Sciences, Materials Sciences and Engineering Division, Mechanical Behavior and Radiation Effects program (FWP 56909) for data collection and analyses using the LEAP 4000X HR. Pacific Northwest National Laboratory is a multiprogram national laboratory operated by Battelle for the U.S. DOE under Contract DE-AC05-79RL01830.

References

[1] B. Gault, M. P. Moody, J. M. Cairney, S. P. Ringer, Atom Probe Microscopy, Vol. 160 of Springer Series in Materials Science, Springer New York, New York, NY, 2012. doi:10.1007/978-1-4614-3436-8.
URL http://link.springer.com/10.1007/978-1-4614-3436-8

[2] D. J. Larson, T. J. Prosa, R. M. Ulfig, B. P. Geiser, T. F. Kelly, Local Electrode Atom Probe Tomography, Springer New York, New York, NY, 2013. doi:10.1007/978-1-4614-8721-0.
URL http://link.springer.com/10.1007/978-1-4614-8721-0_5http://link.springer.com/10.1007/978-1-4614-8721-0

[3] M. K. Miller, R. G. Forbes, Atom-Probe Tomography, Springer US, Boston, MA, 2014. doi:10.1007/978-1-4899-7430-3.
URL http://link.springer.com/10.1007/978-1-4899-7430-3

[4] W. Lefebvre-Ulrikson, F. Vurpillot, X. Sauvage, Atom Probe Tomography, Elsevier, Cambridge, MA, 2016. doi:10.1016/B978-0-12-804647-0.01001-9.

[5] D. Saxey, Correlated ion analysis and the interpretation of atom probe mass spectra, Ultramicroscopy 111 (6) (2011) 473–479. doi:10.1016/j.ultramic.2010.11.021.
URL https://linkinghub.elsevier.com/retrieve/pii/S0304399110003116

[6] D. Santhanagopalan, D. K. Schreiber, D. E. Perea, R. L. Martens, Y. Janssen, P. Khalifah, Y. S. Meng, Effects of laser energy and wavelength on the analysis of LiFePO4 using laser assisted atom probe tomography, Ultramicroscopy 148 (2015) 57–66. doi:10.1016/j.ultramic.2014.09.004.
URL https://linkinghub.elsevier.com/retrieve/pii/S0304399114001752

[7] K. Kruska, D. K. Schreiber, Background Recovery through the Quantification of Delayed Evaporation Multi-Ion Events in Atom-Probe Data, Microsc. Microanal. 21 (S3) (2015) 857–858. doi:10.1017/S1431927615005085.
URL https://academic.oup.com/mam/article/21/S3/857/6954056

[8] B. Gault, D. W. Saxey, M. W. Ashton, S. B. Sinnott, A. N. Chiaramonti, M. P. Moody, D. K. Schreiber, Behavior of molecules and molecular ions near a field emitter, New J. Phys. 18 (3) (2016) 033031. doi:10.1088/1367-2630/18/3/033031.
URL https://iopscience.iop.org/article/10.1088/1367-2630/18/3/033031

[9] E. Di Russo, I. Blum, J. Houard, G. Da Costa, D. Blavette, L. Rigutti, Field-Dependent Measurement of GaAs Composition by Atom Probe Tomography, Microsc. Microanal. 23 (6) (2017) 1067–1075. doi:10.1017/S1431927617012582.
URL https://academic.oup.com/mam/article/23/6/1067/6896971

[10] D. Zanuttini, I. Blum, L. Rigutti, F. Vurpillot, J. Douady, E. Jacquet, P.-M. Anglade, B. Gervais, Simulation of field-induced molecular dissociation in atom-probe tomography: Identification of a neutral emission channel, Phys. Rev. A 95 (6) (2017) 061401. doi:10.1103/PhysRevA.95.061401.
URL http://link.aps.org/doi/10.1103/PhysRevA.95.061401

[11] E. D. Russo, I. Blum, J. Houard, M. Gilbert, G. Da Costa, D. Blavette, L. Rigutti, Compositional accuracy of atom probe tomography measurements in GaN: Impact of experimental parameters and multiple evaporation events, Ultramicroscopy

187 (2018) 126–134. doi:10.1016/j.ultramic.2018.02.001.
URL https://linkinghub.elsevier.com/retrieve/pii/S0304399117304655

[12] I. Blum, L. Rigutti, F. Vurpillot, A. Vella, A. Gaillard, B. Deconihout, Dissociation Dynamics of Molecular Ions in High dc Electric Field, J. Phys. Chem. A 120 (20) (2016) 3654–3662. doi:10.1021/acs.jpca.6b01791.
URL https://pubs.acs.org/doi/10.1021/acs.jpca.6b01791

[13] Z. Peng, D. Zanuttini, B. Gervais, E. Jacquet, I. Blum, P.-P. Choi, D. Raabe, F. Vurpillot, B. Gault, Unraveling the Metastability of C n 2+ (n = 2–4) Clusters, J. Phys. Chem. Lett. 10 (3) (2019) 581–588. doi:10.1021/acs.jpclett.8b03449.
URL https://pubs.acs.org/doi/10.1021/acs.jpclett.8b03449

[14] E. Di Russo, I. Blum, I. Rivalta, J. Houard, G. Da Costa, F. Vurpillot, D. Blavette, L. Rigutti, Detecting Dissociation Dynamics of Phosphorus Molecular Ions by Atom Probe Tomography, J. Phys. Chem. A 124 (52) (2020) 10977–10988. doi:10.1021/acs.jpca.0c09259.
URL https://pubs.acs.org/doi/10.1021/acs.jpca.0c09259

[15] F. Chabanais, E. Di Russo, A. Karg, M. Eickhoff, W. Lefebvre, L. Rigutti, Behavior of the ϵ-Ga 2 O 3 :Sn Evaporation During Laser-Assisted Atom Probe Tomography, Microsc. Microanal. 27 (4) (2021) 687–695. doi:10.1017/S1431927621000544.
URL https://academic.oup.com/mam/article/27/4/687/6888039

[16] D. Zanuttini, I. Blum, L. Rigutti, F. Vurpillot, J. Douady, E. Jacquet, P.-M. Anglade, B. Gervais, Electronic structure and stability of the SiO2+ dications produced in tomographic atom probe experiments, J. Chem. Phys. 147 (16) (oct 2017). doi:10.1063/1.5001113.
URL https://pubs.aip.org/jcp/article/147/16/164301/77148/Electronic-structure-and-stability-of-the-SiO2

[17] D. Zanuttini, F. Vurpillot, J. Douady, E. Jacquet, P.-M. Anglade, B. Gervais, Dissociation of GaN2+ and AlN2+ in APT: Electronic structure and stability in strong DC field, J. Chem. Phys. 149 (13) (oct 2018). doi:10.1063/1.5036933.
URL https://pubs.aip.org/jcp/article/149/13/134310/196995/Dissociation-of-GaN2-and-AlN2-in-APT-Electronic

[18] D. Zanuttini, I. Blum, E. di Russo, L. Rigutti, F. Vurpillot, J. Douady, E. Jacquet, P.-M. Anglade, B. Gervais, Dissociation of GaN2+ and AlN2+ in APT: Analysis of experimental measurements, J. Chem. Phys. 149 (13) (oct 2018). doi:10.1063/1.5037010.
URL https://pubs.aip.org/jcp/article/149/13/134311/196963/Dissociation-of-GaN2-and-AlN2-in-APT-Analysis-of

[19] K. Meng, T. M. Schwarz, E. M. Weikum, P. Stender, G. Schmitz, Frozen n -Tetradecane Investigated by Cryo-Atom Probe Tomography, Microsc. Microanal. 28 (4) (2022) 1289–1299. doi:10.1017/S143192762101254X.
URL https://academic.oup.com/mam/article/28/4/1289/6995608

[20] Z. Peng, F. Vurpillot, P.-P. Choi, Y. Li, D. Raabe, B. Gault, On the detection of multiple events in atom probe tomography, Ultramicroscopy 189 (2018) 54–60. doi:10.1016/j.ultramic.2018.03.018.
URL https://linkinghub.elsevier.com/retrieve/pii/S0304399117305272

[21] K. Thompson, D. Lawrence, D. Larson, J. Olson, T. Kelly, B. Gorman, In situ site-specific specimen preparation for atom probe tomography, Ultramicroscopy 107 (2-3) (2007) 131–139. doi:10.1016/j.ultramic.2006.06.008.
URL https://linkinghub.elsevier.com/retrieve/pii/S0304399106001203

[22] R. Smith, J. M. Walls, Ion trajectories in the field-ion microscope, J. Phys. D. Appl. Phys. 11 (4) (1978) 409–419. doi:10.1088/0022-3727/11/4/005.
URL https://iopscience.iop.org/article/10.1088/0022-3727/11/4/005

[23] A. Cerezo, T. J. Godfrey, S. J. Sijbrandij, G. D. W. Smith, P. J. Warren, Performance of an energy-compensated three-dimensional atom probe, Rev. Sci. Instrum. 69 (1) (1998) 49–58. doi:10.1063/1.1148477.
URL http://aip.scitation.org/doi/10.1063/1.1148477

[24] S. T. Loi, B. Gault, S. P. Ringer, D. J. Larson, B. P. Geiser, Electrostatic simulations of a local electrode atom probe: The dependence of tomographic reconstruction parameters on specimen and microscope geometry, Ultramicroscopy 132 (2013) 107–113. doi:10.1016/j.ultramic.2012.12.012.
URL https://linkinghub.elsevier.com/retrieve/pii/S0304399112002999

[25] I. Corral, A. Palacios, M. Yáñez, Electronic structure and lifetimes of GaX2+ (X = N, O, F) in the gas phase. Unraveling stability trends, Phys. Chem. Chem. Phys. 13 (41) (2011) 18365. doi:10.1039/c1cp21534e.
URL http://xlink.rsc.org/?DOI=c1cp21534e

[26] I. Corral, A. Palacios, M. Yáñez, On the stability and lifetime of GaO2+ in the gas phase, Theor. Chem. Acc. 129 (3-5) (2011) 401–407. doi:10.1007/s00214-010-0863-y.
URL http://link.springer.com/10.1007/s00214-010-0863-y

[27] F. Vurpillot, S. Parviainen, F. Djurabekova, D. Zanuttini, B. Gervais, Simulation tools for atom probe tomography: A path for diagnosis and treatment of image degradation, Mater. Charact. 146 (2018) 336–346. doi:10.1016/j.matchar.2018.04.024.
URL https://linkinghub.elsevier.com/retrieve/pii/S104458031830367X

[28] C. Bacchi, G. Da Costa, F. Vurpillot, Spatial and Compositional Biases Introduced by Position Sensitive Detection Systems in APT: A Simulation Approach, Microsc. Microanal. 25 (2) (2019) 418–424. doi:10.1017/S143192761801629X.
URL https://academic.oup.com/mam/article/25/2/418/6887581

[29] P. Mazzolini, Z. Fogarassy, A. Parisini, F. Mezzadri, D. Diercks, M. Bosi, L. Seravalli, A. Sacchi, G. Spaggiari, D. Bersani, O. Bierwagen, B. M. Janzen, M. N. Marggraf, M. R. Wagner, I. Cora, B. Pécz, A. Tahraoui, A. Bosio, C. Borelli, S. Leone, R. Fornari, Silane-Mediated Expansion of Domains in Si-Doped κ-Ga 2 O 3 Epitaxy and its Impact on the In-Plane Electronic Conduction, Adv. Funct. Mater. 33 (2) (jan 2023). doi:10.1002/adfm.202207821.
URL https://onlinelibrary.wiley.com/doi/10.1002/adfm.202207821

[30] D. Das, F. Sanchez, D. J. Barton, S. Tan, V. Shutthanandan, A. Devaraj, C. V. Ramana, Rationally Engineered Vertically Aligned β -Ga 2- x W x O 3 Nanocomposites for Self-Biased Solar-Blind Ultraviolet Photodetectors with Ultrafast Response, Adv. Mater. Technol. 8 (15) (aug 2023). doi:10.1002/admt.202300014.
URL https://onlinelibrary.wiley.com/doi/10.1002/admt.202300014

[31] B. Mazumder, J. Sarker, Probing structural and chemical evolution in (AlxGa1-x)2O3 using atom probe tomography: A review, J. Mater. Res. 36 (1) (2021) 52–69. doi:10.1557/s43578-020-00072-7.
URL https://link.springer.com/10.1557/s43578-020-00072-7

[32] S.-H. Kim, S. Bhatt, D. K. Schreiber, J. Neugebauer, C. Freysoldt, B. Gault, S. Katnagallu, Understanding atom probe's analytical performance for iron oxides using correlation histograms and ab initio calculations, New J. Phys. 26 (3) (2024) 033021. doi:10.1088/1367-2630/ad309e.
URL https://iopscience.iop.org/article/10.1088/1367-2630/ad309e